

Preparation and physicochemical characterization of α -Fe₂O₃ nanoparticles via sol-gel method

Suresh Sagadevan^{a*}

^aNanotechnology & Catalysis Research Centre, University of Malaya, Kuala Lumpur 50603, Malaysia

Abstract: α -Fe₂O₃ nanoparticles were synthesized using the sol-gel method. The X-ray diffraction (XRD) pattern was used to determine the structure of α -Fe₂O₃ nanoparticles. The presence of α -Fe₂O₃ nanoparticles was confirmed by the FT-IR spectrum. The fact about the surface morphology of α -Fe₂O₃ nanoparticles was revealed by Scanning Electron Microscopic analysis. Transmission Electron Microscopy was used to measure the particle size of the α -Fe₂O₃ nanoparticles. The absorption and photoluminescence (PL) spectrum made it possible to analyze the optical properties of α -Fe₂O₃ nanoparticles. This work was carried to the study of dielectric properties such as the dielectric loss, the dielectric constant, and the AC conductivity of α -Fe₂O₃ nanoparticles, at varied frequencies and temperatures. The magnetic properties of the α -Fe₂O₃ nanoparticles were also investigated.

Keywords: α -Fe₂O₃ nanoparticles, XRD, FT-IR, SEM, TEM, and PL

1. Introduction

The synthesis of inorganic nanoparticles having homogeneous size and shape have been attracted much attention because of the advanced physical and chemical properties [1]. From the past few years, many researchers have been directing their energies towards developing and improving the properties of magnetic nanomaterials [2-6]. The synthesis conditions of the particles must be well controlled to obtain fine powders with the desired narrow particle size distribution and crystallinity. Hematite (α -Fe₂O₃) is the most stable iron oxide under ambient conditions with n-type semiconducting properties ($E_g = 2.1$ eV). Due to its broad commercial and industrial applications in many fields, it has kindled much interest, for instance, catalytic agents, magnetic recording materials, gas sensors, lithium-ion batteries, and drug delivery [7-11]. This paper focuses on α -Fe₂O₃ nanoparticles synthesis using the sol-gel method and their characterization by means of powder X-ray diffraction, Scanning Electron Microscopy (SEM), FTIR, EDX, Transmission Electron Microscope (TEM), UV-analysis, PL, along with the determination of the dielectric properties and magnetic behaviour of α -Fe₂O₃ nanoparticles.

* Corresponding author: drsureshnano@gmail.com

2. Experimental procedure

2.1 Synthesis of α -Fe₂O₃ nanoparticles

α -Fe₂O₃ nanoparticles were synthesized via the sol-gel technique. Typical synthetic procedures required analytical grade 0.15 M of ferric nitrate (Fe(NO)₃·9H₂O) that was dissolved in 50 ml of ethylene glycol (C₂H₆O₂) at 50 °C. To make a stable sol, the solution was vigorously stirred using a magnetic stirrer at the same temperature for 90 minutes. The sol was heated further and the temperature was maintained at 80 °C and stirred continuously until a brown semi-solid (gel) was formed. The gel was dried at 100 °C in a hot air oven for 5 hours and the final product was crushed to powder. The Schematic representation for the synthesis of α -Fe₂O₃ nanoparticles as shown in Fig.1

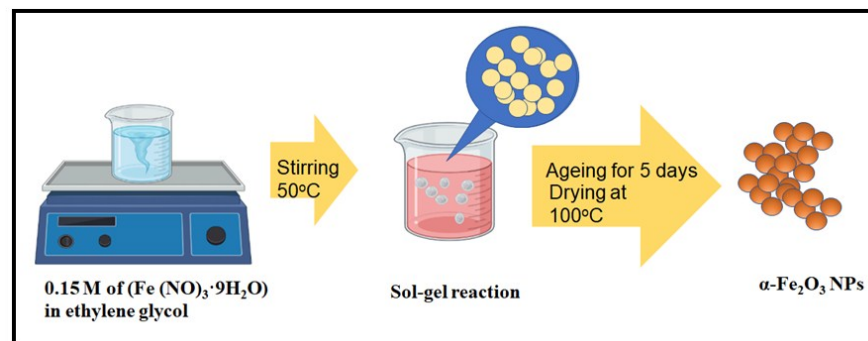


Fig.1 Schematic representation for the synthesis of α -Fe₂O₃ nanoparticles

2.2 Characterization Techniques

The XRD pattern of the α -Fe₂O₃ nanoparticles was recorded by using a powder X-ray diffractometer {Schimadzu model: XRD 6000 using CuK α (λ =0.154 nm) radiation}, with a diffraction angle between 20° and 70°. The FTIR spectrum of the α -Fe₂O₃ nanoparticles were taken using an FTIR model Bruker IFS 66W Spectrometer. SEM study was carried out using JEOL, JSM- 67001. UV-Vis absorption spectrum for the α -Fe₂O₃ nanoparticles were recorded using a Varian Cary 5E spectrophotometer in the range of 400-800 nm. The photoluminescence (PL) spectrum of the α -Fe₂O₃ nanoparticles were recorded using the Perkin-Elmer lambda 900 spectrophotometer with a Xe lamp as the excitation light source. The dielectric properties of the α -Fe₂O₃ nanoparticles was analyzed using a HIOKI 3532-50 LCR HITESTER over the frequency range 50Hz-5MHz. The magnetic behavior of α -Fe₂O₃ nanoparticles was investigated using VSM (Lakeshore VSM 7410).

3. Results and Discussion

3.1 XRD analysis

The powder XRD pattern of α -Fe₂O₃ nanoparticles is shown in Figure 2 where the

peaks are observed at the diffraction planes of (012), (110), (113), (202), (024), (116), (118), (214) and (300), respectively. The observation of such diffraction planes corresponds to the highly crystalline nature of α -Fe₂O₃ NPs. At the rhombohedral structure of hematite α -Fe₂O₃ where all the diffraction peaks were indexed and were in good agreement with JCPDS 86-0550. The sharp diffraction peaks indicates the good crystallinity of the sample. The indication of high purity for as-obtained α -Fe₂O₃ samples was noted as there were no traces of other phases of Fe₂O₃ in the XRD patterns. The average crystalline size of α -Fe₂O₃ NPs was calculated using the Debye Scherrer equation as shown in Eq. (1),

$$D = K \lambda / \beta \cos \theta \quad (1)$$

D is the crystallite size (nm), λ is the wavelength of X-rays (0.15406 Å), α is the full width at half the maximum diffraction peak (FWHM) in radians, and K is the Scherrer constant with a value in the range of 0.9 to 1. The average grain size for the α -Fe₂O₃ NP synthesized was around 33.58 nm.

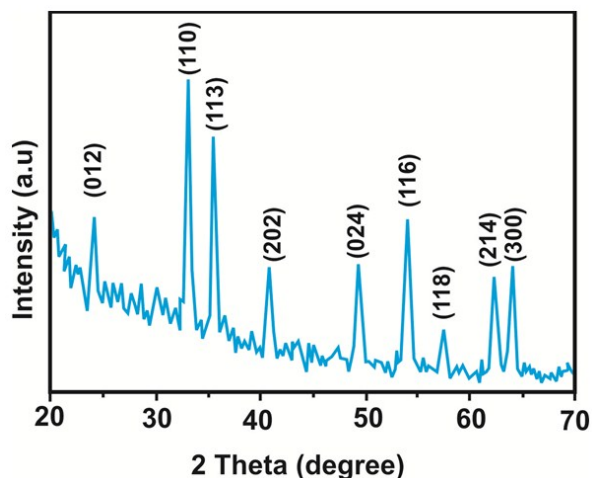


Fig.2 XRD pattern of α -Fe₂O₃ nanoparticles

3.2 FTIR analysis

The functional groups present in the material could be identified using FT-IR. Fig.3 shows the FT-IR transmittance spectrum of α -Fe₂O₃ nanoparticles recorded at room temperature, in the frequency range 500-4000 cm⁻¹. The characteristic absorption peak at 552 cm⁻¹ shows the presence of Fe-O particle. Due to O-H stretching vibration the broad peak exists around 3300 cm⁻¹ and the O-H deformation band corresponds to the one at 1396 cm⁻¹. In OH- groups the O-H stretching vibration is attributed to the large broadband at 3398 cm⁻¹. The symmetric and asymmetric bending vibrations of C=O lead to the absorption around at 1604 cm⁻¹, 1487 cm⁻¹. At 576 cm⁻¹ the band is seen which corresponds to the Fe-O stretching mode of Fe₂O₃. In the sample, the presence of adsorbed water molecule (H-O-H) is the reason for the peak at 1562 cm⁻¹ [12, 13].

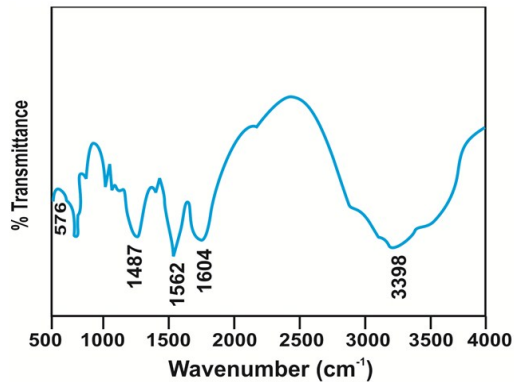


Fig.3 FTIR spectrum of α -Fe₂O₃ nanoparticles

3.3. SEM analysis

The morphology and the size distribution of the α -Fe₂O₃ nanoparticles were determined using SEM. Typical SEM images of α -Fe₂O₃ synthesized particles are shown in Fig.4. As the nanoparticles possess high surface energies, they tend to agglomerate and grow into larger assemblies. The agglomeration of particles while drying is a problem in magnetic nanoparticles systems [14]. In this figure, the particles are prepared with the formation of clusters. The Fe₂O₃ nanocrystals formed were agglomerated. Through the SEM analysis, the rod-like shaped particles with clumped distributions are visible. The particle size was measured to be about 18 nm of as-prepared Fe₂O₃ nanoparticles. The EDX spectrum shown in Fig. 4 indicates Fe and O elements in the Fe₂O₃ compound.

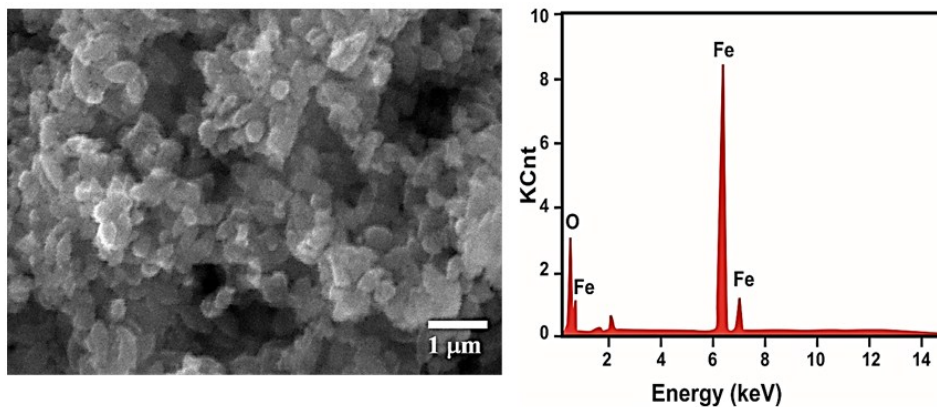


Fig.4 SEM image of α -Fe₂O₃ nanoparticles and EDX spectrum of α -Fe₂O₃ nanoparticles

3.4 Optical Properties

UV-Vis absorption spectral study helped in understanding the electronic structure of the optical bandgap of the material. UV-Vis absorption spectrum of α -Fe₂O₃ nanoparticles is depicted in Fig.5. The characteristic absorption peak is noted near the visible region at around 480 nm. In the UV region the α -Fe₂O₃ nanoparticles exhibit strong absorption

and at 400– 800 nm of the visible region shows weak absorption. Two kinds of electronic transition mechanisms are mainly attributed to the two types of optical absorptions in the UV and visible regions. The former is due to the contribution of the direct charge transition of $O_2^- 2p \rightarrow Fe^{3+} 3d$ (UV absorption), and the latter originates from the indirect charge transition of $Fe^{3+} 3d \rightarrow 3d$ (visible absorption) [15]. The band-gap energy (E_g) value of the prepared α -Fe₂O₃ nanoparticles was derived from the relationship between the absorption coefficient and the incident photon energy of the α -Fe₂O₃ nanoparticles using Tauc's plot method. For the direct allowed transition, Fig.6 shows the Tauc plot (the linear extrapolation of $(\alpha h\nu)^2$ versus $h\nu$ to the energy axis) of α -Fe₂O₃ nanoparticles. The value given for bulk Fe₂O₃ is 2.2 eV where the average band gap energy has come out from the Tauc plot as 2.6 eV and found to be greater as in comparison. The value obtained for the bandgap is 2.6 which is in good agreement with the reported value of 2.58 [16, 17]. Thus, relative to the peak absorption of bulk Fe₂O₃ there is a blue shift. This is because of the quantum confinement effect where delocalized electronic states are close to the Fermi level [18, 19].

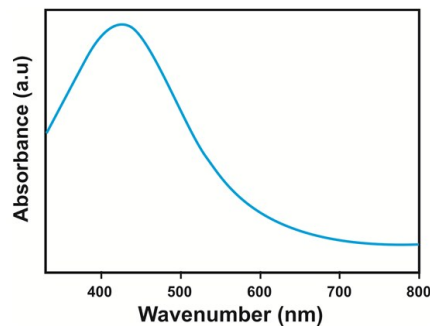


Fig.5 UV-Vis absorbance spectrum of α -Fe₂O₃ nanoparticles

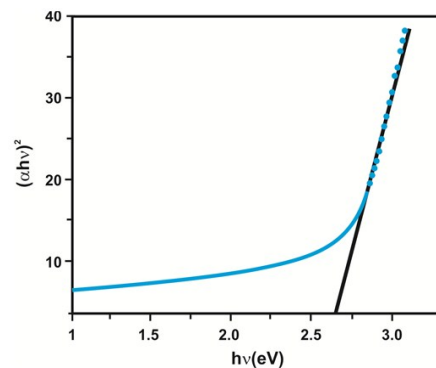


Fig.6 plot of $(\alpha h\nu)^2$ versus $h\nu$

Fig.7 shows the photoluminescence spectrum of α -Fe₂O₃ nanoparticles. Photoluminescence spectrum displays peak around 630 nm and emission which appears as a fine structure on the higher energy side. Due to the band-edge emission of the α -Fe₂O₃ nanoparticles, the broad and intense PL peak is at \sim 630 nm, which corresponds to indirect and direct transitions to the band-gap energies of 1.9 eV.

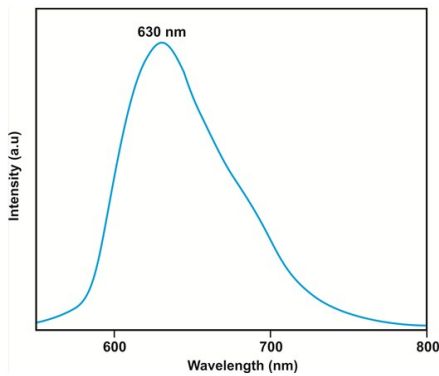


Fig. 7 PL spectrum of α - Fe_2O_3 nanoparticles

3.5 Dielectric Properties

The α - Fe_2O_3 nanoparticle pellets in disk form were studied at different temperatures. For measurements, the samples were obtained with a diameter of ~ 10 mm and thickness ~ 1 mm, and a sample was placed between the electrodes having a conventional four-terminal sample holder for investigations involving temperature variations along with a conventional two-terminal sample holder for ambient conditions alone. The sample was mounted between copper platforms and electrodes. To ensure good electrical contact, the faces were coated with silver paint. The capacitance and the dissipation factor of the parallel plate capacitor which was formed by the copper plate and the electrode having the sample as a dielectric medium were measured. The fact that electric field allocation within the α - Fe_2O_3 nanoparticles was given by the analysis of the dielectric nature of α - Fe_2O_3 nanoparticles. At various temperatures in Fig.8 and 9, the frequency reliance of the dielectric constant and the dielectric loss are shown respectively. It was observed to exhibit the similar nature in both dielectric constant and dielectric loss. On the contribution of electronic, ionic, bipolar, and space charge polarization of the frequencies the dielectric constant of materials depends [20]. At low frequencies all four polarization mechanisms are active. The progress of space charge polarization is normally assisted by the lower frequencies and high temperatures. At the lower frequency range, the loose or weak bond of ions is the reason for the low value of the dielectric constant with increasing frequency [21]. Due to the charge accumulation at the grain boundaries still higher values of the dielectric constant are possible at low frequencies. To gain higher values is another possibility due to the heterogeneous dielectric structure that possesses the interfacial/space charge polarization. It was observed that as the frequency beyond a certain frequency of the external field increased, the polarization decreased and then reached a constant value; this could be explained by the hopping between various metal ions that could not follow the alternating field. It was noticed that with an increase in the frequency the value of the dielectric constant decreased [22]. The energy dissipation in the dielectric system is represented by the dielectric loss. With the frequency at various temperatures, Fig.9 shows the variation in the dielectric loss factor. It was observed that the dielectric loss acquired a low value in the high-frequency region

and with the increase in frequency, the dielectric loss decreased. From the study, it was shown that at lower frequencies the dielectric loss suddenly fell and at higher frequencies, constant nature was noticed. Due to the space charge polarization, it was observed that for all temperatures, with the increase in frequency the dielectric loss decreased [23, 24].

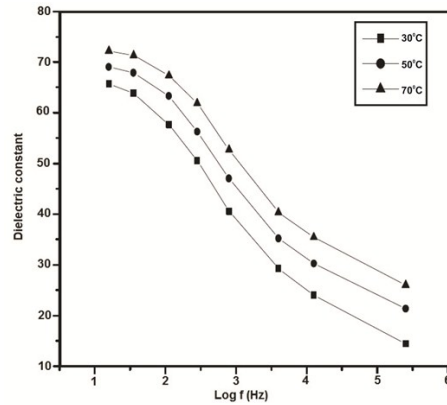


Fig.8 Dielectric constant plot for α -Fe₂O₃ nanoparticles

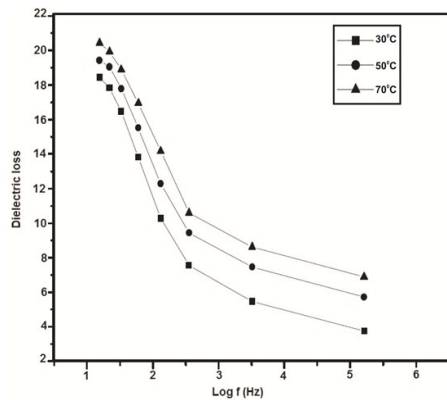


Fig.9 Dielectric loss plot for α -Fe₂O₃ nanoparticles

3.6. AC Conductivity studies

The AC conductivity of the α -Fe₂O₃ nanoparticles, could be calculated by using the following relation:

$$\sigma_{ac} = 2\pi\epsilon_0\epsilon_r f \tan \delta \quad (2)$$

where ϵ_0 is permittivity in free space, ϵ_r is dielectric constant, f is the frequency, and $\tan \delta$ is the loss factor. Due to electrons jumping in the metal ions from a low valence state to high valence state the electrical conduction in α -Fe₂O₃ nanoparticles took place. In the temperature interval between 30°C to 70°C the frequency reliance behaviour for the ac conductivity is shown in Fig.10. The ac conductivity increased with the increase

in frequency for all temperatures. With the increase in the frequency of the applied ac field, it was observed that the ac conductivity gradually increased due to the electron hopping frequency. The increase in conductivity could be caused by a reduction in space charge polarization with higher frequencies.

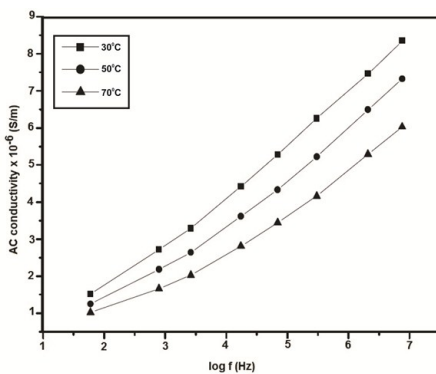


Fig.10 AC conductivity plot for α -Fe₂O₃ nanoparticles

3.7 Magnetic measurements

The magnetic behavior of α -Fe₂O₃ nanoparticles was investigated. The origin of high coercivity values was due to the slower rate of growth of crystallite size that took place during the heating process. Apart from the temperature, the magnetic spin orientation along the axis that eases magnetization attributed by morphology also plays a significant role in the magnetic properties and the increased coercivity value [25]. The magnetic properties got enhanced due to the grain boundaries and free surface [26]. Fig.11 shows at room temperature the magnetic hysteresis loops of the α -Fe₂O₃ nanoparticles. The magnetic parameters, namely retentivity, coercivity, and saturation magnetization of the sample were measured to be 3882 G, 0.152 emu/g, and 0.325 emu/g respectively.

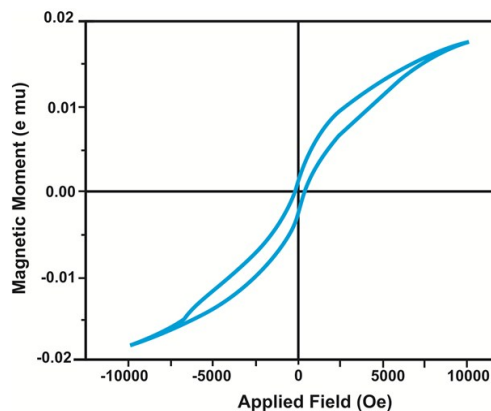


Fig.11 Hysteresis loop of α -Fe₂O₃ nanoparticles

4. Conclusion

The paper briefly discussed the employment of the sol-gel method for the synthesis of α -Fe₂O₃ nanoparticles. With the help of the XRD and SEM analysis the fact that the α -Fe₂O₃ nanoparticles belonged to the rhombohedral structure was established. The formation of α -Fe₂O₃ nanoparticles was also supported by the FTIR spectrum. The SEM analysis established the fact that nanoparticles agglomerated to form rod-like shaped particles with clumped distributions are visible. The α -Fe₂O₃ nanoparticles' average particle size was found to be 24 nm. The optical properties were studied with the help of UV-Visible absorption spectrum and PL spectrum. The optical band gap for α -Fe₂O₃ nanoparticles was found to be 2.6 eV. The fact that the prepared α -Fe₂O₃ nanoparticles exhibited the broad blue-green emission band centered at 630 nm was confirmed by the PL spectrum. Analysis with respect to varying dielectric constant, the dielectric loss, and the AC conductivity with frequency and temperature was performed for α -Fe₂O₃ nanoparticles. From the studies of α -Fe₂O₃ nanoparticles dielectric properties it became clear that both the dielectric constant and the dielectric loss decreased with an increase in the frequency. With an increase in the temperature and the frequency, the AC electrical conductivity was found to increase. The VSM measurements were used to determine magnetic properties.

Conflict of interest:

The author declare no conflict of interest with this work.

Acknowledgments:

The author would like to acknowledge the financial support provided by a Research University grant from University of Malaya (RU001-2020).

References

- [1] T.P.Almeida, M.Fay, Y.Q.Zhu, P.D.J.Brown, *Phys Chem C*, 113(2009)18689-98.
- [2] S. Saravanakumar, R. Saravanan, S. Sasikumar, *Chem.Pa.*, 68 (2014) 788-797.
- [3] F. Sánchez-DeJesús, A.M. Bolarín-Miró, C.A. Cortés-Escobedo, R. Valenzuela, S.Ammar, *Ceram. Int*, 140 (2014) 4033-4038.
- [4] A. Zelenakova, V. Zelenak, S. Michalik, J. Kovac, M.W. Meisel, *Phys. Rev. B* 89 (2014)104417.
- [5] S.I. Srikrishna Ramya, C.K. Mahadevan, *J. Solid State Chem*, 211 (2014) 37-50
- [6] H. Liang, X. Xu, W. Chen, B. Xu, Z. Wang, *CrystEngComm*, 16 (2014) 959-963.
- [7] S.H.Jiao, Y.Chen, X.Man, Y.W.Zhang, D.Wang, G.S.Pang, *Mater Lett*, 64(2010)1704-6.
- [8] S.Y.Zeng, K.B.Tang, W.J. LiT, *Colloid Interface Sci*, 312(2007)513-52.
- [9] C.Z.Wu, P.Yin, X.Zhu, C.Z.OuYang, Y.J. Xie, *PhysChemB*, 110(2006)17806-12.
- [10] B.Sun, J. Horvat, H.S.Kim, W.S.Kim, J.H.Ahn, G.X.J.Wang, *Phys Chem C*, 114(2010)18753
- [11] Y.Chen, H.R.Chen, D.P.Zeng, Y.B.Tian, F.Chen, J.W.Feng, *ACS Nano*, 4(2010)6001-13.
- [12] N.J.English, M. Rahman, N. Wadnerkar and J.M.D. MacElroy, *Phys. Chem. Chem. Phys.*, 16 (2014) 14445-14454.
- [13] S.B. Lima, S.M.S. Borges, M.C. Rangel, S.G. Marchetti, *J. Braz. Chem. Soc*, 24 (2013)344

- [14] X.Weï, R.C. Viadero Jr, *Coll. Surf. A: Physicochem. Eng. Asp.* 294(2007) 280
- [15] Z. Zhang, T. Takahashi, and M. F. Hossain, *Materials Letters*, 64(2010) 435–438
- [16] Khosro Zangeneh Kamali, Pandikumar Alagarsamy, NayMing Huang, Boon Hoong Ong, and Hong Ngee Lim, *The Scientific World Journal*, 2014, Article ID 396135, 13 pages
- [17] B.K.Pandey, A.K. Shahi, J.Shah, R.K.Kotnala, R.Gopal, *Appl Surf Sci* 289(2014) 462
- [18] B. Gilbert, C. Frandsen, E.R. Maxey and D.M. Sherman, *Phys. Rev. B*, 79 (2009) 035108.
- [19] X.G. Wen, S.H. Wang, Y. Ding, Z.L. Wang, S.H. Yang, *J. Phys. Chem., B.*, 109 (2005) 215–220.
- [20] S. Suresh, C. Arunseshan, *Appl Nanoscience*, 4 (2014)179–184
- [21] Sagadevan Suresh, *Appl Nanoscience*, 4(2014)325–329
- [22] Suresh Sagadevan, *American Journal of Nanoscience and Nanotechnology*, 1(2013)27-30
- [23] Sagadevan Suresh, *International journal of Physical Sciences*, 8(2013) 1121-1127
- [24] S Sagadevan, *Journal of Nano Research*, 34 (2015)91-97
- [25] X. Zhang, Y. Niu, Y. Li, X. Hou, Y. Wang, R. Bai, J. Zhao, *Mater. Lett.*, 99 (2013) 111–114.
- [26] B.B.Straumal, A.A.Mazilkin, S.G.Protasova, A.A.Myatiev, P.B.Straumal, E.Goering, *Thin Solid Films*, 520(2011) 1192-4



This document was created with the Win2PDF "print to PDF" printer available at <http://www.win2pdf.com>

This version of Win2PDF 10 is for evaluation and non-commercial use only.

This page will not be added after purchasing Win2PDF.

<http://www.win2pdf.com/purchase/>